Biosensors and Bioelectronics 169 (2020) 112616

Contents lists available at ScienceDirect

Biosensors and Bioelectronics

journal homepage: http://www.elsevier.com/locate/bios

A thermophoresis–based biosensor for real–time detection of inorganic phosphate during enzymatic reactions

Peter Franz [a], Vincent Gassl [a], Andrea Topf [a], Luca Eckelmann [b], Bogdan Iorga [b,c], Georgios Tsiavaliaris [a,*]

[a] Cellular Biophysics, Institute for Biophysical Chemistry, OE 4350, Hannover Medical School, 30625, Hannover, Germany
[b] Institute for Molecular and Cell Physiology, Hannover Medical School, Hannover, Germany
[c] Department of Physical Chemistry, Faculty of Chemistry, University of Bucharest, Bucharest, Romania

ARTICLE INFO

Keywords:
Phosphate sensor
Phosphate binding protein
Thermophoresis
Enzyme catalysis
Myosin
Myofibrils

ABSTRACT

Inorganic phosphate (P_i)–sensing is a key application in many disciplines, and biosensors emerged as powerful analytic tools for use in environmental P_i monitoring, food quality control, basic research, and medical diagnosis. Current sensing techniques exploit either electrochemical or optical detection approaches for P_i quantification. Here, by combining the advantages of a biological P_i–receptor based on the bacterial phosphate binding protein with the principle of thermophoresis, *i.e.* the diffusional motion of particles in response to a temperature gradient, we developed a continuous, sensitive, and versatile method for detecting and quantifying free P_i in the subnanomolar to micromolar range in sample volumes $\leq$10 μL. By recording entropy–driven changes in the directed net diffusional flux of the P_i–sensor in a temperature gradient at defined time intervals, we validate the method for analyzing steady–state enzymatic reactions associated with P_i liberation in real–time for adenosine triphosphate (ATP) turnover by myosin, the actomyosin system and for insoluble, high molecular weight enzyme–protein assemblies in biopsy derived myofibrils. Particular features of the method are: (1) high P_i–sensitivity and selectivity, (2) uncoupling of the read–out signal from potential chemical and spectroscopic interferences, (3) minimal sample volumes and nanogram protein amounts, (4) possibility to run several experiments in parallel, and (5) straightforward data analysis. The present work establishes thermophoresis as powerful sensing method in microscale format for a wide range of applications, augmenting the current set of detection principles in biosensor technology.

1. Introduction

Common methods for studying enzyme activities are mainly spectroscopy–based, enabling real–time detection of catalytic turnover directly by monitoring changes in fluorescence or absorbance associated with product formation. Beside colorimetric assays, which utilize chemical dyes to quantify product concentration (Martinez Gache et al., 2020; He and Honeycutt, 2005; Fiske and Subbarow, 1925; Briggs, 1922, 1924), biosensors (Okoh et al., 2006) and coupled enzyme systems (Sehgal et al., 2016; Ingerman and Nunnari, 2005; Hinman and Blass, 1981; McClure, 1969; Kaltwasser and Schlegel, 1966) have become standard tools for assessing enzymatic activities (Nayak et al., 2020). Of particular importance is the detection of inorganic phosphate (P_i), which is liberated as hydrolysis product during the catalysis reactions of various nucleotide-dependent enzymes involved in regulating cell metabolism, DNA replication or signaling (Dick et al., 2011; Hunter, 1995; Shenolikar, 1994), including motor proteins that act as force generators and transducers converting chemical energy into mechanical work (Kaya et al., 2017; Lionne et al., 2003). The molybdenum blue method (Murphy and Riley, 1958) and the malachite green assay (Van Veldhoven and Mannaerts, 1987) are routinely used in various analytical disciplines to quantify P_i concentrations; however, a major obstacle of the techniques is that they are restricted to fixed time–point measurements and chemicals like silica, arsenate, carboxylic acids, and detergents often interfere with accuracy of the measurement (Sarwar et al., 2019).

Protein–coupled assays based on native and genetically modified bacterial periplasmic–binding proteins (bPBPs) have emerged as complementary methods for P_i–detection (Mukherjee et al., 2015; Lionne et al., 1995; Brune et al., 1994). Fluorescent tagging converts this family

* Corresponding author. Georgios Tsiavaliaris Institute for Biophysical Chemistry, Hannover Medical School Carl-Neuberg-Str. 1, 30625, Hannover, Germany.
E-mail address: tsiavaliaris.georgios@mh-hannover.de (G. Tsiavaliaris).

https://doi.org/10.1016/j.bios.2020.112616
Received 30 July 2020; Received in revised form 9 September 2020; Accepted 13 September 2020
Available online 16 September 2020

of proteins into sensitive and highly selective P_i–sensors, capable of detecting picomole quantities of inorganic phosphate for use in various applications ranging from P_i–concentration determination in environmental probes, cells and tissues, to quantitative measurements of catalytic turn–over of enzymatic reactions (de Lorimier et al., 2002). Despite the potential of the method to probe almost any biochemical reaction producing phosphate, the fluorescence–based detection represents a major limitation, since pH, ionic strength, and temperature can influence sensitivity (Kanno et al., 2016), while additional factors like fluorescence quenching and auto–fluorescence may interfere with the detection signal. Moreover, enzymatic activities of macromolecular protein complexes are often difficult to be assessed by the method, since scattering contributes to signal disturbances (Simeonov and Davis, 2004). Real-time radioisotope imaging, $^{31}P_i$–nuclear magnetic resonance (NMR), Secondary Ion Mass Spectrometry (SIMS), Inductively Coupled Plasma-Atomic Emission Spectroscopy (ICP-AES), Mass Spectrometry (ICP-MS), and chemoelectrical biosensors (Kanno et al., 2016) have gained increasing importance for quantifying P_i, however, their adaptation for use in enzymatic reactions remains still challenging (Lawal and Adeloju, 2013).

Alternatively, continuous assays employing a nicotinamide adenine dinucleotide hydride (NADH)–coupled nucleotide regeneration system have been developed to quantify nucleotide turn–over rates (Sehgal et al., 2016; Ingerman and Nunnari, 2005). Two subsequent enzymatic reactions couple nucleoside diphosphate production to NADH oxidation, yielding a spectroscopic signal that reports the steady–state kinetics of the hydrolysis reaction of interest. Compared to phosphate sensors, the NADH–coupled assay, however, is less sensitive and protein consuming, particularly for enzymatic reactions with generally low turnover rates (Radnai et al., 2019). Moreover, since nucleotides are quantified and not P_i, the assay is unsuitable for reactions, in which nucleotides are not set free but incorporated, like during DNA replication and RNA transcription by polymerases or upon the action of nucleotidyl transferases (Cramer, 2019).

To overcome the limitation of electrochemical and optical P_i–sensing, we developed a method that is based on monitoring thermophoresis, also known as the Ludwig-Soret effect (Duhr and Braun, 2006). By exploiting the P_i–binding capacity of the bacterial phosphate binding protein (PBP) and its ability to undergo conformational transition upon P_i–binding, we achieved to quantify P_i by tracing the relative changes in directional diffusion of the P_i–receptor in a thermal gradient. The method provides an improvement in selectivity compared to colorimetric assays, allowing continuous and quantitative P_i–monitoring with high sensitivity in the low part per billion ranges than classical fluorescence and absorbance–based techniques. A major advantage of the thermodiffusion–based detection in microscale format is the ultralow protein consumption in applications addressing catalytic activities of enzymes.

2. Experimental section

2.1. Materials

Expression plasmid pPBPΔsigS234C, encoding N–terminally truncated phosphate binding protein (PBP) from *E. coli* with mutation S234C and a C-terminal Hexa–His–tag, was obtained by two subsequent PCR reactions using cDNA from the *E. coli* strain *LK111λ*. Primer pair 5′–TTTGGATCCATGGAAGCAAGCCTGACAGGTGC–3′ and 5′–TTTTGCGGCCGCTTATT ATGTACACTCGAGGTACAGCGGCTTACC GCTAC–3′ were used to amplify the gene lacking the N-terminal periplasmic translocation sequence. The PCR product was subsequently cloned into the pET23a vector using BamHI/XhoI restriction sites. Site-directed mutagenesis with primer pair 5′–TCAGGATCTGACCAACC AGAAAGGCGAAGATGCA–3′ and 5′–GCGAAGGTTTTGCACCAGTCT GCACCTTTTGCTGCATTAGCGAAGTTTTCTTCG–3′ led to the final expression plasmid verified by sequencing.

Expression plasmid pPBPΔsigS234C was transformed into chemocompetent Rosetta (DE3)pLysS cells. Bacteria were grown on lysogeny broth (LB)–Agar plates supplemented with 100 μg/ml ampicillin and 30 μg/ml chloramphenicol at 37 °C overnight. A single colony was inoculated in 100 ml LB–medium supplemented with the same antibiotics and grown under at 37 °C overnight. The culture was diluted in 2 l and grown to optical density (OD) at 600 nm OD_{600nm} = 0.8–1 following addition of 0.4 mM isopropyl β–D–1–thiogalactopyranoside (IPTG) and incubation at 37 °C for 3 h. Cells were harvested by centrifugation (5000×*g*, 10 min, 4 °C) and resuspended in 50 ml lysis buffer containing 50 mM tris(hydroxymethyl)aminomethane (Tris–HCl) pH = 7.6, 5 mM 2–mercaptoethanol, protease inhibitor cocktail (Roche: 11873580001), and flash frozen in liquid nitrogen and stored at −80 °C. Cells were thawed on ice and sonicated 5 times for 2 min (50% duty cycle, 50% amplitude). Whole cell lysate was centrifuged at 30 krpm (Ti45 rotor; Beckman Coulter) at 4 °C for 1 h. Supernatant was applied to a nickel nitrilotriacetic acid (NiNTA)–chromatography column using the ÄKTA pure system (GE Healthcare). Washing was performed with 200 ml Tris–HCl buffer (20 mM; pH = 7.6) and 200 ml Tris–HCl buffer containing 300 mM NaCl. The protein was eluted using Tris–HCl buffer (pH = 7.6) containing 500 mM imidazole by applying a 4 column volume gradient. Eluted fractions contained 300 mg total protein. Protein fractions were concentrated to >100 mg/ml using a 10 k MWCO cut–off Vivaspin 20 Ultrafiltration Unit (Sartorius), dialyzed two times in 1 l Tris–HCl buffer (20 mM, pH = 7.5), and applied to size exclusion chromatography (Superdex S75 26/60 pg, GE Healthcare) using Tris–HCl buffer (20 mM; 50 mM NaCl, pH = 7.6). Pure protein fractions were concentrated to ~3 mM (molar extinction coefficient at 280 nm: ε_{280nm} = 61,880 $M^{-1}cm^{-1}$; molar mass: M_w = 37 kDa), flash frozen in liquid nitrogen as 20 μl aliquots, and stored at −80 °C. For fluorescence labeling, a 100 μM PBP-S234C solution was incubated with 150 μM Atto 655–maleimide (Merck) in Tris–HCl buffer (20 mM; pH = 7.5) at room temperature for 1 h. Excess dye was removed by size exclusion chromatography (Superdex S75 16/60 pg, GE Healthcare; Tris–HCl buffer; 20 mM; 50 mM NaCl; pH = 7.5). Labelling efficiency was determined photometrically by calculating the ratio of total protein concentration and dye concentration using ε_{663nm} = 125,000 $M^{-1}cm^{-1}$ (for Atto655 dye) and the correction factor 0.08 at 280 nm. Labeled protein was flash frozen in liquid nitrogen and stored at −80 °C.

D. discoideum (*Dd*) myosin-2 motor domain fragment was prepared as described (Tsiavaliaris et al., 2002). Actin was prepared from chicken as described (Pardee and Aspudich, 1982).

Cardiac myofibrils from the left ventricle of the pig heart (pvMFs) were prepared in rigor as it follows: myocardial samples were dissected from the left ventricle of a pig heart, quickly frozen, minced into small sizes like resulting from tiny biopsies, and stored for long term in liquid nitrogen. One–to–three frozen small myocardial samples were first incubated for maximum 10 min (~2 min at room temperature, then <8 min on ice) in a fast–rigor buffer [10 mM imidazole, pH = 7.0 at ~5 °C, 5 mM ethylene glycol-bis(β-aminoethyl ether)-N,N,N′,N’-tetraacetic acid (EGTA), 12 mM ethylenediamine tetraacetic acid (EDTA), 30 mM 2,3–butanedione monoxime (BDM), 10 mM caffeine, 115 mM potassium propionate, 5 mM 1,4–dithiothreitol (DTT), protease inhibitor cocktail (PIC) composed of 10 μM leupeptin, 1 μg/ml aprotinin, 10 μM antipain, 10 μM E64, 1 mM 4–(2–aminoethyl)benzenesulfonyl fluoride hydrochloride (AEBSF)]. Samples were then incubated for 30 min in ice-cold rigor buffer supplemented with 1% TritonX–100 to demembranate myocardial samples, while the sarcomeric structure is still preserved (Iorga et al., 2018). Samples were twice washed with the same buffer solution without TritonX–100 for 10 min on ice to remove detergent. Finally, samples were transferred in the rigor buffer containing 10 mM imidazole, 2.5 mM EGTA, 2.5 mM EDTA, 150 mM potassium propionate, 5 mM DTT and PIC (pH 7.0 at 5 °C), and washed two times for 15–20 min. Samples were rapidly homogenized within 7–8 s using an Ultra-Turrax homogenizer at maximum speed (>25,000 rpm) with a 5 mm rotor diameter (IKA® T10 basic). Myofibrils suspension was then

filtered through a mesh with a pore size of 2 1 μm to remove large aggregates. The final myofibrillar stock solution was kept on ice and used within three days. Before use, myofibrils were thoroughly mixed with a pipette to obtain a homogeneous solution. The average sarcomeric length of freshly prepared and stored myofibrils in rigor state was between 1.9 and 2.1 μm, as for relaxed cardiac myofibrils.

The concentration of β–cardiac myosin from myofibril preparations was determined densitometrically. In particular, a reference solution of purified pig full–length β–cardiac myosin with the myosin light chains MLC–1 and MLC–2 of known concentration calculated from the theoretically determined $\varepsilon_{280nm} = 226{,}000\ M^{-1}cm^{-1}$ based on the amino acid sequence of the 524 kDa protein using Expasy protparam tool (Wilkins et al., 1999). Defined amounts (0.1–1.5 μg) of pig full-length β–cardiac myosin were applied to an 8% sodium dodecyl sulfate–polyacrylamide gel electrophoresis (SDS-PAGE) and stained with Coomassie after electrophoresis. A calibration line was obtained by plotting band intensity (quantified using the ImageJ "measure tool") vs protein amount. Whole myofibrillar samples were applied to SDS-PAGE and β–cardiac myosin band intensities were related to protein concentration following the calibration procedure. Additionally, the absorption of the samples was measured and a calibration line determined correlating protein amount to optical density at 280 nm (OD_{280}). An OD_{280} of 1 corresponds to a β–cardiac myosin concentration of 49.3 ± 6.9 μg/ml. The linear relationship enables direct determination of β–cardiac myosin concentration present in pvMFs preparations from the optical density at 280 nm (OD_{280}).

2.2. Methods

The experiments were performed in a Microscale Themorphoresis (MST) device from NanoTemper Technologies GmbH. Prior to each experiment, P_i contaminations were removed using a P_i–mop based on purine nucleoside phosphorylase (PNPase) and 7-methyl-guanosine (7-MEG), Merck KGaA. In brief, 5x-adenosine triphosphate (ATP) assay buffer composed of 125 mM 4-(2-hydroxyethyl)-1-piperazineethanesulfonic acid (HEPES), 125 mM KCl, 25 mM $MgCl_2$, pH 7.3), 5x-pvMF buffer (125 mM HEPES, 250 mM KCl, 25 mM $MgCl_2$, 5 mM EGTA, pH 7.3), were supplemented with 2x experimental buffers containing 0.2 mM 7-MEG, 0.5 U/ml PNPase, 0.1% Tween–20 and 2 mM DTT. Subsequently, a sensor mix containing 50 nM $PBP^{Atto655}$, 100 μM $PBP^{unlabeled}$, 4 mM ATP in 1x experimental buffer was prepared and incubated for 30 min at room temperature. For MST–experiments, the P_i–mop was inactivated by the addition of forodesine-HCl (50 μM final concentration; MedChemExpress). P_i–affinity to PBP-S234C was determined by filling capillaries (purchased from NanoTemper Technologies GmbH) with equal amounts of sensor mix (5 μl) and K_2HPO_4 (5 μl) to obtain final P_i–concentrations of 0.1 μM–250 μM. For ATPase measurements, a defined myosin solution or pvMFs suspension was prepared corresponding to 1x experimental buffers supplemented with 200 μM forodesine–HCl and incubated at room temperature for 30 min. Reaction was started with the addition of 6 μl sensor mix to a 1:1 mixture of 3 μl myosin solution or pvMFs suspension and 3 μl 1x experimental buffer and immediately filled into capillaries. Actin- and Ca^{2+}-activated ATPase measurements were performed by mixing 6 μl sensor mix with 3 μl myosin solution or pvMFs suspension and 3 μl actin (20 μM, 40 μM in 1x experimental buffer) or $CaCl_2$ solution (4 mM, 8 mM in 1x experimental buffer), respectively. Experiments were performed with the Monolith NT.115 pico device (Nanotemper) at 25 °C, 4% LED-power (red filter set) and 60% MST–power. NADH–coupled assays were performed using 200 nM *Dd* myosin and 100 nM β–cardiac myosin following the procedures as described (Fujita-Becker et al., 2006) using a BioTek microplate reader.

2.3. Data analysis

Primary data of P_i–titration experiments were exported and analyzed using the Origin2018b software (Originlab). Average ± SD F_{norm} values from 3 individual measurements were plotted against the corresponding P_i–concentrations and data were fitted according to equation (1), which describes the average number of ligands bound to a receptor for binding equilibrium, where Min and Max define the minimum and maximum F_{norm} amplitude values corresponding to 0 and 100% P_i–bound $PBP^{Atto655}$. K_D is the equilibrium dissociation constant, P_0 and L_0 represent initial PBP and P_i concentrations, respectively. n is the Hill-coefficient.

$$F_{norm} = Min + (Max - Min)\cdot\frac{\left\{\frac{1}{K_D}\cdot\left(L_0 - \frac{K_D+P_0+L_0}{2} + \sqrt{\left(\frac{K_D+P_0+L_0}{2}\right)^2 - P_0\cdot L_0}\right)\right\}^n}{1+\left\{\frac{1}{K_D}\cdot\left(L_0 - \frac{K_D+P_0+L_0}{2} + \sqrt{\left(\frac{K_D+P_0+L_0}{2}\right)^2 - P_0\cdot L_0}\right)\right\}^n} \quad (1)$$

Data from ATPase measurements were globally fitted using equation (2), which is a modification of equation (1), in which the ligand concentration L_0 is replaced by the product of time t [s] and reaction rate v [μM/s] to consider time–dependent changes in ligand concentration (L_0) that occur during the reaction. Data form three independent experiments were averaged and errors calculated as standard deviation (SD).

$$F_{norm} = Min + (Max - Min)\cdot\frac{\left\{\frac{1}{K_D}\cdot\left(v\cdot t - \frac{K_D+P_0+v\cdot t}{2} + \sqrt{\left(\frac{K_D+P_0+v\cdot t}{2}\right)^2 - P_0\cdot v\cdot t}\right)\right\}^n}{1+\left\{\frac{1}{K_D}\cdot\left(v\cdot t - \frac{K_D+P_0+v\cdot t}{2} + \sqrt{\left(\frac{K_D+P_0+v\cdot t}{2}\right)^2 - P_0\cdot v\cdot t}\right)\right\}^n} \quad (2)$$

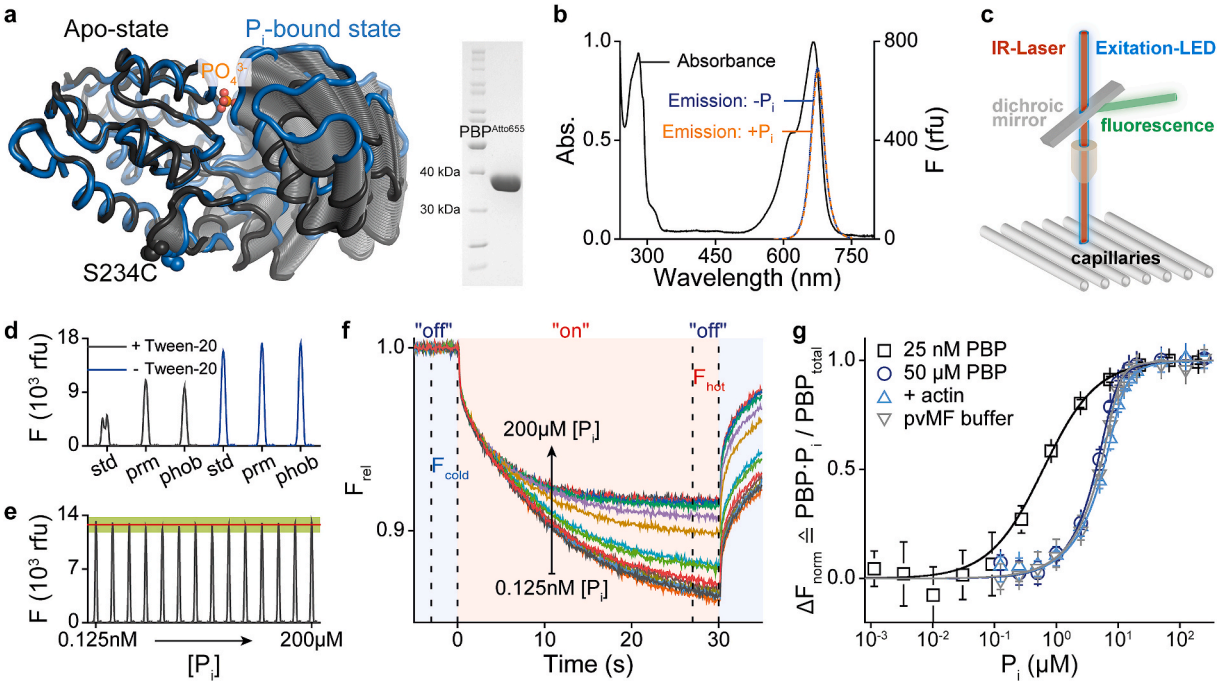

Fig. 1. Thermophoresis-based P_i–detection. **a,** Superimposed X-ray structures of the P_i–receptor PBP in the P_i–free (apo, PDB: 1OIB) and P_i–bound state (PDB: 2ABH). P_i–binding induces structural rearrangements and rigid body motions (interpolated trajectories). Mutation S234C enabled site-specific fluorescent labeling. The purity of Atto 655–labeled PBP-S234C ($PBP^{Atto655}$) is shown by SDS-PAGE. **b,** Normalized absorption spectrum (black line) of $PBP^{Atto655}$ and corresponding fluorescence spectra of the P_i–bound (blue, dashed line) and P_i–free (blue, dotted line) state of the protein shown as relative fluorescence units (rfu). **c,** Schematic illustration of the MST setup. The P_i–sensor is filled into chemically functionalized glass capillaries. Thermophoresis is initiated by the induction of a temperature gradient of 2–6 °C using a focused IR–laser beam. Directional movements are monitored by detecting local changes in fluorescence. **d,** Sample fluorescence profiles in different capillaries in the absence and presence of detergent. Standard capillaries (std), premium capillaries (prm), hydrophobic capillaries (phob) as provided by NanoTemper. The capillaries contain a solution of sensor mix (5 µl) and K_2HPO_4 (5 µl) in the presence and absence of 0.05% Tween–20 (for detailed composition of reaction mixture see also Methods). **e**, Sample fluorescence profiles of $PBP^{Atto655}$ in the presence of increasing amounts of P_i. **f,** Multi–capillary P_i–titration experiment. Normalized fluorescence traces reporting the thermophoretic behavior of $PBP^{Atto655}$ molecules in the presence of increasing P_i–concentrations (colored lines). Colored areas highlight the time periods before induction of a temperature gradient (blue), during heating (red), and after switching–off the IR–laser (blue). **g**, P_i–concentration dependence of sensor–thermophoresis at different experimental conditions. Changes in thermophoresis (ΔF_{norm}) follow hyperbolic dependencies reporting the fraction of P_i–bound PBP.

Data analysis and graphical representation of results were done with Origin 8.0 (OriginLab Corporation, U.S.A.). The non-linear least square fitter of Origin 8.0 was used for global data analysis. Equation (1) was implemented as user defined function to the fit. Global fit included three experimental data sets sharing the same parameters that were implemented either as fixed values (min; max; K_D) or free values (P_0). The function was written in the script form of the software to allow assignment of the independent variables *t* and *v*. Additionally, experimental errors were included to the fit as statistical weighting parameters. The global fit analysis was performed several times with different initial guesses of parameters to avoid solutions which could correspond to local minima of fit.

3. Results and discussion

3.1. Design and performance of the thermophoresis–based P_i–sensor

For enabling P_i–detection by thermophoresis, we exploited the intrinsic property of PBP to undergo a conformational transition upon P_i–binding (Wang et al., 1994) (Fig. 1a). P_i–free (apoPBP) and P_i–bound PBP ($PBP{\cdot}P_i$) are thus expected to differ in their thermodiffusional movements as a consequence of changes in surface area and hydration entropy. To monitor the thermophoretic movements, we fluorescently labeled a mutant version of PBP (S234C) with the fluorescent dye Atto 655–maleimide. The domain in which the label was attached undergoes only minor conformational changes upon P_i–binding. This guarantees sensing is realized only via changes in thermodiffusion (Jerabek-Willemsen et al., 2014). The almost indistinguishable emission spectra of P_i–bound and P_i–free $PBP^{Atto655}$ demonstrate that this requirement is fulfilled (Fig. 1b).

Using a Microscale Thermophoresis (MST) device (Jerabek-Willemsen et al., 2011) equipped with microliter capillaries, an infrared (IR)-laser for inducing thermophoresis, light-emitting diodes (LEDs) with optical filters for sample excitation, and a detector system for tracking thermophoretic movements (Fig. 1c), we evaluated the P_i–sensing ability of $PBP^{Atto655}$ in P_i–titration experiments under different conditions. Prior to the experiments, buffer solutions, proteins, and chemicals were treated with a phosphate mop (P_i–mop) based on purine nucleoside phosphorylase (PNPase) and 7-methylguanosine (7-MEG) to remove contaminant traces of inorganic phosphate. Subsequently, the P_i–mop was inactivated by the addition of forodesine to prevent P_i depletion during the measurements (Alonso et al., 2009; Balakrishnan et al., 2006). An important requirement in assessing the thermophoretic behavior of molecules is that the detection signal remains stable over time (Jerabek-Willemsen et al., 2014). This was achieved with standard-coated capillaries containing 25 nM $PBP^{Atto655}$ in buffer supplemented with Tween–20 (Fig. 1d and e). Under these conditions, the P_i–dependent thermophoretic behavior of $PBP^{Atto655}$ could be reproducibly recorded for different buffers and experimental conditions yielding homogenous and constant fluorescent signals up to 200 µM P_i concentrations (Fig. 1f). The observed amplitude decrease in the thermophoretic traces with increasing P_i reflects the degree of PBP saturation.

Table 1
P_i–binding capability of the MST-based P_i–sensor.

Conditions	$K_D/10^{-9}$ mol l^{-1}	n	$P_0/10^{-6}$ mol l^{-1}	R^2
25 nM $PBP^{Atto655}$	600 ± 32	1.0 ± 0.1	0.025	0.996
25 nM $PBP^{Atto655}$/50 μM PBP	582 ± 197	1.1 ± 0.1	7.6 ± 0.6	0.997
+ actin	634 ± 120	1.0 ± 0.1	10.2 ± 0.4	0.999
+ pvMF buffer	277 ± 95	1.0 ± 0.1	9.5 ± 0.3	0.998

P_0: total PBP concentration in assay.
n : Hill coefficient.
R^2: coefficient of determination.

Plots of the fluorescent amplitudes (F_{norm}) vs P_i concentration revealed hyperbolic dependencies (Fig. 1g) that could be described by equation (1), yielding equilibrium dissociation constants (K_D) of complex formation consistent with those described in the literature (Sippel et al., 2014; Okoh et al., 2006; Wang et al., 1994; Brune et al., 1994). Additives like protein polymers and salt had no detectable influence on the sensitivity of the P_i–sensor. Also P_i–titrations performed under second order conditions with respect to PBP concentration yielded reproducible K_D values (Table 1). The results confirmed the high sensitivity of the biosensor for performing P_i–analyses.

3.2. Real-time quantification of P_i production during enzymatic ATP turnover

To probe the performance of the P_i–sensor in assessing catalytic turn–over rates of enzymatic reactions of solubilized proteins in assay buffer, we used the well–established acto–myosin system, which catalyzes the hydrolysis of ATP to P_i and adenosine diphosphate (ADP) (Fig. 2a). By accelerating product release, filamentous actin acts as exchange factor increasing the myosin ATPase by several orders of magnitude (Diensthuber et al., 2015; Fedorov et al., 2009; Taft et al., 2008). Using a mixture of $PBP^{Atto655}$ (25 nM)/$PBP^{unlabeled}$ (50 μM) and small amounts of myosin (≤1 μg), we were able to resolve the ATPase reaction of a recombinant myosin construct in the absence and presence of actin in a single capillary. The addition of excess amounts of unlabeled PBP was necessary to ensure that PBP·P_i complex formation progressed faster than the actual rate of ATP turn over by myosin. This is of critical importance particularly for the initial stages of the ATPase reaction, where total P_i concentrations range below the K_D of the PBP·P_i equilibrium. In repetitive scans of the same capillary, we monitored a decrease in the thermophoretic amplitudes (Fig. 2b) that correlates to the degree of PBP·P_i complex formation ($PBP^{Atto655}$·P_i/PBP_{total}) at defined time-points and consequently to the rate of P_i–production (Fig. 2c). Global non–linear least square fitting of the hyperbolic time–dependencies of PBP·P_i complex formation using equation (2), yielded ATP turnover rates that resembled in good agreement those obtained from reference experiments using the NADH–coupled assay, which assesses ADP (Fig. 2c, inset).

Further, by scanning several capillaries simultaneously, we demonstrated the reproducibility of the method, while reducing total experimental time. Overall, the method is an improvement over standard spectrophotometry–based assays, like the NADH–coupled enzyme system, which required 20–fold higher total protein amounts, even when performed in the 96–well format using a multi–plate reader (Fig. 2c inset; Table 2). The time scale of acquisition is suitable for assessing the kinetic parameters of steady–state reactions. In our experiments, the time scale of P_i–release by myosin is in the one hundredth to tenth of second range and thus fast enough to detect all released P_i. However, when studying slower enzymatic reactions, total acquisition time should be adjusted accordingly.

3.3. Quantification of myofibrillar ATPase activity

Besides applying this method to low concentrations of P_i–releasing soluble enzymes, we were interested also to test whether this method can assess P_i resulting from ATPase activities of few protein–clusters, each containing high local concentrations of P_i–releasing enzymes. Such question makes sense because a major challenge in studying enzymes is the investigation of their performances in the context of ordered structures with physiological relevance. In this superior three–dimensional organization multiple collective interactions, including those influenced by accessory and regulatory proteins, can significantly modulate the catalytic activities of the enzymes of interest. Such highly ordered structures can be found for example, in striated muscles (Walcott et al., 2012). Inside cardiac and skeletal muscle cells, assemblies of myofibrils (MFs), each consisting in a serial repetitive arrangement of sarcomeric units that are composed of interdigitating thick (myosin) and thin (actin) filaments packed at high density, drive muscle contraction, while hydrolyzing the ATP (Fig. 3a).

Current methods for studying in real–time the steady–state ATPase of the myosin motors within myofibrils (Okafor et al., 2003; Lionne et al., 2003; Alousi et al., 1990) are difficult for analyses when only small samples are available. Such investigations are relevant for addressing the molecular basis of disease–related mutations in sarcomeric proteins causing cardiomyopathies and muscle disorders (de Winter and Ottenheijm, 2017; Kraft et al., 2013). Modest amounts of myofibrillar samples can be derived usually from human muscle biopsies (Askew et al., 2010; Kentish and Stienen, 1994), or found in single contractile cell models (Montag et al., 2018), in pluripotent stem cell–derived cardiomyocytes (Iorga et al., 2018) and in small model organisms such as zebrafish larvae (Iorga et al., 2011).

Here, the low volume requirements, continuity, and sensitivity of our MST–method allowed us determine quantitatively the ATPase activity of relaxed and Ca^{2+}–activated pvMFs. The β–cardiac myosin content of myofibrils was determined densitometrically by SDS–PAGE using purified β–cardiac myosin as reference material (Fig. 3b) and correlated upon calibration to the optical density of myofibril suspension (Fig. 3c). Minimal amounts of myofibrils, equivalent to 13, 26, and 52 ng β–cardiac myosin, were sufficient to monitor the time course of P_i production in the absence (Fig. 3d) and presence of Ca^{2+} (Fig. 3e) as a function of $PBP^{Atto655}$·P_i/PBP_{total} and calculate ATP turnover rates

Table 2
Performance of the MST–based P_i–sensor in myosin ATPase reactions.

Myosin head fragment (myosin)					
Concentrations/mass		Fitting parameters		ATPase/s^{-1}	
[Myosin]/10^{-9}mol l^{-1} (10^{-9}g)	[Actin]/10^{-6}mol l^{-1} (10^{-6}g)	v/10^{-9}mol $l^{-1}s^{-1}$	R^2	MST	NADH
50 (58)	0 (0)	3.1 ± 0.1	>0.98	0.06 ± 0.01	n.a.
	5 (2)	12.1 ± 1.6	>0.97	0.24 ± 0.03	n.a.
	10 (4)	22.1 ± 2.3	>0.93	0.44 ± 0.05	n.a.
200 (1160)	0 (0)	n.a.		–	0.06 ± 0.01
	5 (10)			–	0.30 ± 0.02
	10 (20)			–	0.50 ± 0.01

v: rate of reaction.
R^2: coefficient of determination.

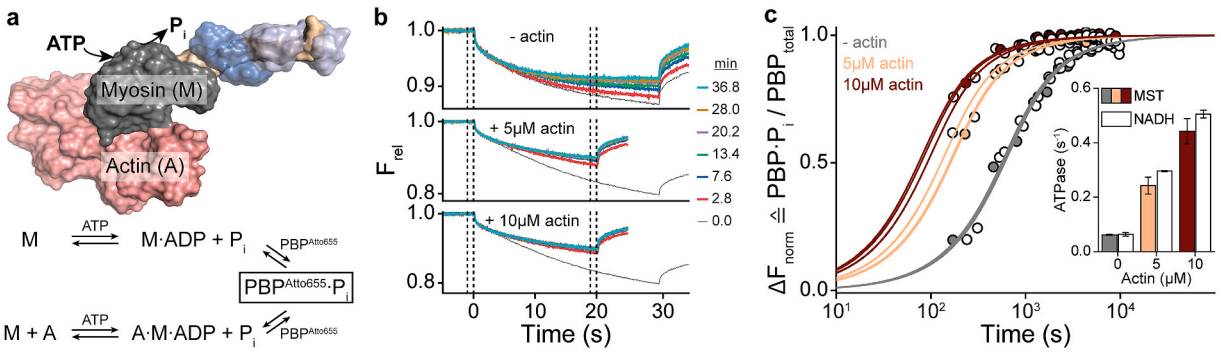

Fig. 2. Real-time quantification of P_i–turnover by the acto-myosin system. **a,** Simplified reaction scheme of the acto–myosin ATPase reaction in the presence of the P_i–sensor $PBP^{Atto655}$. **b**, Time–dependent fluorescence profiles of the thermophoretic behavior of $PBP^{Atto655}$ during the myosin ATPase reaction in the absence or presence of actin. The acquisition time points for each scan are shown as inset. The grey lines show fluorescence profiles in the absence of myosin (zero time point). Dotted lines indicate fluorescence time intervals that were used for calculating the corresponding F_{norm} values. As the ATPase reaction proceeds, the amplitude of the thermophoretic signal decreases, indicating an increase of the PBP·P_i fraction. **c,** Real–time detection of P_i production during the myosin ATPase. Data points represent saturation kinetics of $PBP^{Atto655}$·P_i complex formation, rate–limited by the basal (grey circles) and actin–activated steady–state ATPase (colored circles) of myosin. Global fit analysis was performed with all data sets according to equation (2), yielding rates of ATP turnover that are in good agreement with those obtained with the NADH–coupled assay (inset). Fitting and kinetic parameters are summarized in Table 2. Results are plotted as mean ± SD from three independent experiments.

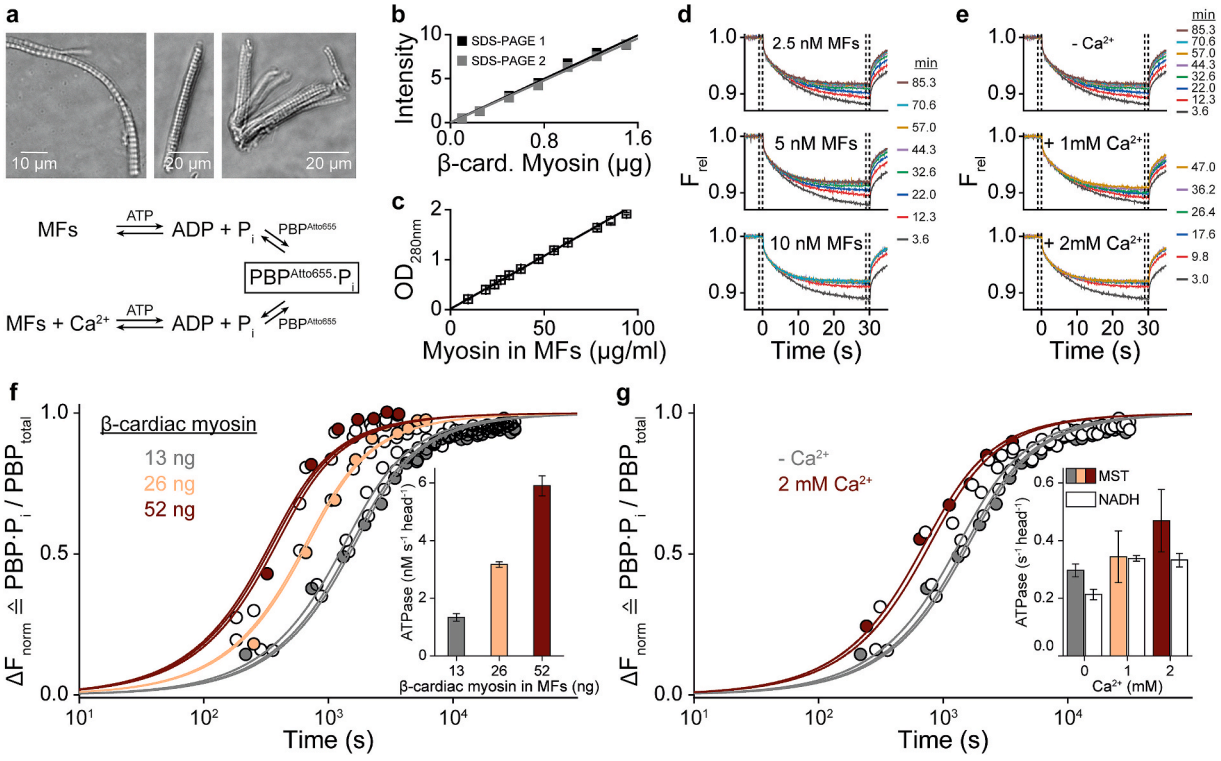

Fig. 3. ATPase measurements with nanogram myofibril quantities. **a,** Microscopic pictures of native pig left ventricular myofibrils, pvMFs (upper panel). Ca^{2+}–free (relaxed) and Ca^{2+}–activated ATPase of pvMFs myofibrils (lower panel) was measured in single capillaries containing different amounts of myofibrils. **b**, Determination of β–cardiac myosin concentration in isolated pvMFs based on densitometric calibration. **c,** Optical density of diluted pvMFs suspensions. **d,e**, Fluorescence recordings of the thermophoretic behavior of $PBP^{Atto655}$ during the ATPase reaction of relaxed (**d**) and Ca^{2+}–activated myofibrils (**e**). As the ATPase reaction progresses, thermophoretic amplitudes decrease relative to the degree of PBP·P_i complex formation. The acquisition time points for each scan are shown as insets. Dotted lines indicate fluorescence time intervals that were used for calculating the corresponding F_{norm} values. **f**, Data points showing time–course of P_i–production during the myofibrilar ATPase reaction as a function of $PBP^{Atto655}$·P_i complex formation. Global fit analysis was performed with all data sets using equation (2), yielding rates of ATP turnover summarized in Table 3. Capillaries contained a few nanograms myofibrils, equivalent to 13, 26, and 52 ng of total β–cardiac myosin content, respectively. Inset shows the corresponding ATP turnover rates for a defined β–cardiac myosin concentration within the myofibrillar suspension. **g**, P_i–production of Ca^{2+}–activated myofibrils as a function of $PBP^{Atto655}$·P_i complex formation. Inset shows Ca^{2+}–activation of the myofibrillar ATPase as obtained by MST and using the NADH–coupled assay. Fitting and kinetic parameters are summarized in Table 3. Results are plotted as mean ± SD of three independent experiments.

Table 3
Sensitivity performance of P_i–sensor in myofibrillar ATPase activity.

Left ventricular myofibrils (pvMfs)

Mass or concentration		Fitting parameter		ATPase/s^{-1}	
β–cardiac myosin/10^{-9}g	$[Ca^{2+}]/10^{-3}$mol l^{-1}	v/10^{-9}mol l^{-1} s^{-1}	R^2	MST	NADH
13	0	1.3 ± 0.1	>0.97	0.28 ± 0.03	n.a.
	1	1.7 ± 0.4	>0.92	0.34 ± 0.09	n.a.
	2	2.3 ± 0.5	>0.93	0.47 ± 0.11	n.a.
26	0	3.2 ± 0.1	>0.98	0.32 ± 0.01	n.a.
52	0	5.9 ± 0.3	>0.91	0.29 ± 0.02	n.a.
1300	0	n.a.		–	0.21 ± 0.02
	1			–	0.31 ± 0.01
	2			–	0.30 ± 0.01

v: rate of reaction.
R^2: coefficient of determination.

following global fitting procedures using equation (2) (Fig. 3f, g). The results are in good agreement with data from reference experiments that we obtained with the NADH-coupled assay (Fig. 3f, inset; Table 3) and match the values described in the literature with multicellular preparations (Kuhn et al., 1990). Our thermophoresis–based approach demonstrates an improvement in amount of biological samples required for determining catalytic activity; in terms of enzyme concentration by approximately one to two orders of magnitude (Tables 2 and 3).

4. Conclusions

Despite the fact that thermophoresis has become a well–established technique to investigate protein–ligand interactions and analyze protein dynamics, its application in quantifying product formation during enzymatic reactions and derive steady–state kinetic parameters has remained yet unexplored (Jerabek-Willemsen et al., 2014). The principle, on which the herein described method builds, couples the entropy–driven thermodiffusional movements of a protein–based P_i–sensor to enzyme–catalyzed nucleotide hydrolysis reactions, enabling real–time quantification of phosphate production. A main aspect is that changes in thermophoretic mobility of the P_i–sensor induced by P_i–binding can directly be correlated to the time course of the hydrolysis reaction, while fluorescent labeling of the P_i–sensor is only required for monitoring the diffusional movements.

We have shown the validity of the thermophoresis–biosensor to measure the ATPase activity of myosin and actin–myosin proteins at very low concentrations and of nanogram quantities of subcellular myofibrils, which is a pertinent amount that can be obtained from muscle biopsies (Borchert et al., 2010). Despite of the economic amount of myofibrils in suspension inside the 10 µl capillary volume, the local concentration of myosin molecules in each sarcomere is similar to that found in striated muscle (Lionne et al., 2003; Tikunov et al., 2001). Such reduction in protein consumption of more than 100–fold compared to other assays, enables new experimental strategies to be further engaged.

Thermodiffusion–based sensing can potentially be realized with any bioreceptor that undergoes changes in mass, size, charge, and/or solvation upon ligand/analyte binding or other interactions affecting the entropy of the system. Thus, the method is applicable to a broad spectrum of targets including metabolites, signaling molecules, and biomarkers, thereby circumventing the problems of optical interferences and signal disturbances that may occur with optical techniques. This suggests that the present method has the potential to enlarge its applicability to accompany for example research efforts towards the design of drug delivery systems and studies of dynamics from molecular or supramolecular ensembles to collective behavior.

In conclusion, the use of the thermophoresis–based P_i–sensor for studying enzyme reactions goes beyond classical techniques and represents a new, simple, and fast analytical tool with high reproducibility for a wide range of interdisciplinary and translational applications.

Funding

This work was supported by the German Research Council (Deutsche Forschungsgemeinschaft, DFG) Research grants TS 169/5–1 to Georgios Tsiavaliaris.

CRediT authorship contribution statement

Peter Franz: Investigation, Methodology, Validation, Formal analysis, Visualization, Writing - original draft, Writing - review & editing. **Vincent Gassl:** Investigation, Formal analysis. **Andrea Topf:** Investigation. **Luca Eckelmann:** Resources. **Bogdan Iorga:** Resources, Methodology, Writing - review & editing. **Georgios Tsiavaliaris:** Conceptualization, Methodology, Project administration, Investigation, Formal analysis, Visualization, Supervision, Writing - original draft, Writing - review & editing, Funding acquisition.

Declaration of competing interest

The authors declare that they have no known competing financial interests or personal relationships that could have appeared to influence the work reported in this paper.

Acknowledgements

We thank Igor Chizhov (Hannover Medical School, Hannover, Germany) and Corinne Lionne (Institut national de la santé et de la recherche médicale, Monpellier, France) for discussions, and Theresia Kraft (Hannover Medical School, Hannover, Germany) for support.

References

Alonso, R., Lopez-Guerra, M., Upshaw, R., Bantia, S., Smal, C., Bontemps, F., Manz, C., Mehrling, T., Villamor, N., Campo, E., Montserrat, E., Colomer, D., 2009. Blood 114, 1563–1575.
Alousi, A.A., Grant, A.M., Etzler, J.R., Cofer, B.R., Van der Bel-Kahn, J., Melvin, D., 1990. Mol. Cell. Biochem. 96, 79–88.
Askew, G.N., Tregear, R.T., Ellington, C.P., 2010. J. Exp. Biol. 213, 1195–1206.
Balakrishnan, K., Nimmanapalli, R., Ravandi, F., Keating, M.J., Gandhi, V., 2006. Blood 108, 2392–2398.
Borchert, B., Tripathi, S., Francino, A., Navarro-Lopez, F., Kraft, T., 2010. Cardiol. J. 17, 518–522.
Briggs, A.P., 1924. J. Biol. Chem. 59, 255–264.
Briggs, A.P., 1922. J. Biol. Chem. 53, 13–16.
Brune, M., Hunter, J.L., Corrie, J.E., Webb, M.R., 1994. Biochemistry 33, 8262–8271.
Cramer, P., 2019. Nature 573, 45–54.
de Lorimier, R.M., Smith, J.J., Dwyer, M.A., Looger, L.L., Sali, K.M., Paavola, C.D., Rizk, S.S., Sadigov, S., Conrad, D.W., Loew, L., Hellinga, H.W., 2002. Protein Sci. 11, 2655–2675.
de Winter, J.M., Ottenheijm, C.A.C., 2017. J. Neuromuscul. Dis. 4, 99–113.
Dick, C.F., Dos-Santos, A.L., Meyer-Fernandes, J.R., 2011. Enzym. Res. 2011, 103980.
Diensthuber, R.P., Tominaga, M., Preller, M., Hartmann, F.K., Orii, H., Chizhov, I., Oiwa, K., Tsiavaliaris, G., 2015. Faseb. J. 29, 81–94.
Duhr, S., Braun, D., 2006. Proc. Natl. Acad. Sci. U. S. A 103, 19678–19682.

Fedorov, R., Bohl, M., Tsiavaliaris, G., Hartmann, F.K., Taft, M.H., Baruch, P., Brenner, B., Martin, R., Knolker, H.J., Gutzeit, H.O., Manstein, D.J., 2009. Nat. Struct. Mol. Biol. 16, 80–88.
Fiske, C.H., Subbarow, Y., 1925. J. Biol. Chem. 66, 375–400.
Fujita-Becker, S., Tsiavaliaris, G., Ohkura, R., Shimada, T., Manstein, D.J., Sutoh, K., 2006. J. Biol. Chem. 281, 36102–36109.
He, Z., Honeycutt, C.W., 2005. Commun. Soil Sci. Plant Anal. 36, 1373–1383.
Hinman, L.M., Blass, J.P., 1981. J. Biol. Chem. 256, 6583–6586.
Hunter, T., 1995. Cell 80, 225–236.
Ingerman, E., Nunnari, J., 2005. Methods Enzymol. 404, 611–619.
Iorga, B., Neacsu, C.D., Neiss, W.F., Wagener, R., Paulsson, M., Stehle, R., Pfitzer, G., 2011. J. Gen. Physiol. 137, 255–270.
Iorga, B., Schwanke, K., Weber, N., Wendland, M., Greten, S., Piep, B., Dos Remedios, C. G., Martin, U., Zweigerdt, R., Kraft, T., Brenner, B., 2018. Front. Physiol. 8, 1111.
Jerabek-Willemsen, M., André, T., Wanner, R., Roth, H.M., Duhr, S., Baaske, P., Breitsprecher, D., 2014. J. Mol. Struct. 1077, 101–113.
Jerabek-Willemsen, M., Wienken, C.J., Braun, D., Baaske, P., Duhr, S., 2011. Assay Drug Dev. Technol. 9, 342–353.
Kaltwasser, H., Schlegel, H.G., 1966. Anal. Biochem. 16, 132–138.
Kanno, S., Cuyas, L., Javot, H., Bligny, R., Gout, E., Dartevelle, T., Hanchi, M., Nakanishi, T.M., Thibaud, M.C., Nussaume, L., 2016. Plant Cell Physiol. 57, 690–706.
Kaya, M., Tani, Y., Washio, T., Hisada, T., Higuchi, H., 2017. Nat. Commun. 8, 16036.
Kentish, J.C., Stienen, G.J., 1994. J. Physiol. 475, 175–184.
Kraft, T., Witjas-Paalberends, E.R., Boontje, N.M., Tripathi, S., Brandis, A., Montag, J., Hodgkinson, J.L., Francino, A., Navarro-Lopez, F., Brenner, B., Stienen, G.J., van der Velden, J., 2013. J. Mol. Cell. Cardiol. 57, 13–22.
Kuhn, H.J., Bletz, C., Ruegg, J.C., 1990. Pflügers Archiv 415, 741–746.
Law al, A.T., Adeloju, S.B., 2013. Talanta 114, 191–203.
Lionne, C., Brune, M., Webb, M.R., Travers, F., Barman, T., 1995. FEBS Lett. 364, 59–62.
Lionne, C., Iorga, B., Candau, R., Travers, F., 2003. J. Muscle Res. Cell Motil. 24, 139–148.
Martinez Gache, S.A., Recoulat Angelini, A.A., Sabeckis, M.L., Gonzalez Flecha, F.L., 2020. Anal. Biochem. 597, 113681.
McClure, W.R., 1969. Biochemistry 8, 2782–2786.
Montag, J., Kowalski, K., Makul, M., Ernstberger, P., Radocaj, A., Beck, J., Becker, E., Tripathi, S., Keyser, B., Muhlfeld, C., Wissel, K., Pich, A., van der Velden, J., Dos Remedios, C.G., Perrot, A., Francino, A., Navarro-Lopez, F., Brenner, B., Kraft, T., 2018. Front. Physiol. 9, 359.
Mukherjee, P., Banerjee, S., Wheeler, A., Ratliff, L.A., Irigoyen, S., Garcia, L.R., Lockless, S.W., Versaw, W.K., 2015. Plant Physiol. 167, 628–638.
Murphy, J., Riley, J.P., 1958. J. Mar. Biol. Assoc. U. K. 37, 9–14.
Nayak, A., Wang, T., Franz, P., Steffen, W., Chizhov, I., Tsiavaliaris, G., Amrute-Nayak, M., 2020. J. Biol. Chem. 295, 7046–7059.
Okafor, C., Liao, R., Perreault-Micale, C., Li, X., Ito, T., Stepanek, A., Doye, A., de Tombe, P., Gwathmey, J.K., 2003. Mol. Cell. Biochem. 245, 77–89.
Okoh, M.P., Hunter, J.L., Corrie, J.E., Webb, M.R., 2006. Biochemistry 45, 14764–14771.
Pardee, J.D., Aspudich, J., 1982. Methods Enzymol. 85, 164–181.
Radnai, L., Stremel, R.F., Sellers, J.R., Rumbaugh, G., Miller, C.A., 2019. JoVE 150. https://doi.org/10.3791/60017.
Sarwar, M., Leichner, J., Naja, G.M., Li, C., 2019. Microsyst. Nanoeng. 5, 56.
Sehgal, P., Olesen, C., Moller, J.V., 2016. Methods Mol. Biol. 1377, 105–109.
Shenolikar, S., 1994. Annu. Rev. Cell Biol. 10, 55–86.
Simeonov, A., Davis, M.I., 2004. Interference with fluorescence and absorbance. In: Sittampalam, G.S., Grossman, A., Brimacombe, K., Arkin, M., Auld, D., Austin, C.P., Baell, J., Bejcek, B., Caaveiro, J.M.M., Chung, T.D.Y., Coussens, N.P., Dahlin, J.L., Devanaryan, V., Foley, T.L., Glicksman, M., Hall, M.D., Haas, J.V., Hoare, S.R.J., Inglese, J., Iversen, P.W., Kahl, S.D., Kales, S.C., Kirshner, S., Lal-Nag, M., Li, Z., McGee, J., McManus, O., Riss, T., Saradjian, P., Trask OJ, J., Weidner, J.R., Wildey, M.J., Xia, M., Xu, X. (Eds.), Assay Guidance Manual, Bethesda (MD).
Sippel, K.H., Bacik, J., Quiocho, F.A., Fisher, S.Z., 2014. Acta Crystallogr. F. Struct. Biol. Commun. 70, 819–822.
Taft, M.H., Hartmann, F.K., Rump, A., Keller, H., Chizhov, I., Manstein, D.J., Tsiavaliaris, G., 2008. J. Biol. Chem. 283, 26902–26910.
Tikunov, B.A., Sweeney, H.L., Rome, L.C., 2001. J. Appl. Physiol. 90, 1927–1935, 1985.
Tsiavaliaris, G., Fujita-Becker, S., Batra, R., Levitsky, D.I., Kull, F.J., Geeves, M.A., Manstein, D.J., 2002. EMBO Rep. 3, 1099–1105.
Van Veldhoven, P.P., Mannaerts, G.P., 1987. Anal. Biochem. 161, 45–48.
Walcott, S., Warshaw, D.M., Debold, E.P., 2012. Biophys. J. 103, 501–510.
Wang, Z., Choudhary, A., Ledvina, P.S., Quiocho, F.A., 1994. J. Biol. Chem. 269, 25091–25094.
Wilkins, M.R., Gasteiger, E., Bairoch, A., Sanchez Jc FAWilliams, K.L., Williams, K.L., Appel, R.D., Hochstrasser, D.F., 1999. Methods Mol. Biol. 112, 531–552.